



X International Conference on Structural Dynamics, EURODYN 2017

Strength demands of tall wind turbines subject to earthquakes and wind load

P. Martinez-Vazquez, M. Gkantou, C. Baniotopoulos

*School of Engineering; Civil Engineering Department, The University of Birmingham, Edgbaston B15 2TT,
Birmingham, United Kingdom*

Abstract

Wind and earthquake load have historically been conceived to act independently. However, if we reflect on the fact that major seismic events are usually followed by a number of aftershocks and that wind is constantly flowing at high intensities around wind farms, which induces additional demands of resistance to infrastructure, then the joint probability of middle-to strong earthquakes and low-to mild wind events becomes more relevant. In this paper a generalised approach is used to estimate the ratio between earthquake and wind forces and their effect on infrastructure. Following, a probabilistic analysis is carried out to show that under certain conditions the combination of these natural events can induce additional demands of strength and ductility to wind turbines which could lead to unforeseen damage.

© 2017 The Authors. Published by Elsevier Ltd.

Peer-review under responsibility of the organizing committee of EURODYN 2017.

Keywords: hyper-tall wind turbines; earthquake and wind load; multi-hazard load scenarios

1. Introduction

In the past decades a number of areas across the world have been identified where the energy production of Class I and Class II wind energy increases exponentially. This is largely due to the availability of natural resources, technological developments and qualified labour. The fast growing of energy generation however requires careful consideration of the type of infrastructure that can fulfil the demands in terms of strength, resilience and innovation. On the other hand, it is acknowledged that in certain regions tectonic and environmental conditions make infrastructure often susceptible to earthquakes and wind effects both during construction and once in operation. Notwithstanding that, current engineering practice disregards their simultaneous occurrence even though past earthquake records show that further ground accelerations can occur within days or even hours from the main event.

Examples of this include the earthquake that hit the Sichuan Province in China in 2008 ($M_s = 7.9$) which was followed by 12 weeks with 42 aftershocks ranging in magnitude between $5 < M_s < 6.4$, killing over 87,000 and leaving over £56bn in losses [1]. The earthquake that hit Nepal in 2015 ($M_s = 7.8$) killing more than 8,000 [2] was followed by 30 aftershocks of $M_s < 5$ occurring within three weeks and killing 200 more. More recently, the earthquakes that hit Ecuador in 2016 ($M_s = 7.8$) killing over 600, were followed by over 55 aftershocks in the first 24 hours [3]. Some attempts to fill in this gap in knowledge have been reported in [4] where it was shown that the combination of earthquakes and wind would decrease the value of strength reduction factors that are calculated by ignoring the impact of wind during earthquake events whilst the joint probability of occurrence of such natural events could not be ignored because it would lead to non-conservative designs. Moreover, in [5] is shown that wind turbines have adequate earthquake resistance provided these are designed against typhoons - which could be the case of offshore units but not a common practice in the case of onshore infrastructure; whilst in [6] is demonstrated that operational earthquake combined with design wind load tend to over-stress the tower section hence increasing the strength demand established under isolated wind conditions. The present paper is therefore concerned with the analysis of strength demands imposed by combinations of earthquake and wind load acting on wind turbines which exceed 150 m height and the associated probabilities of such multi-load scenarios.

2. Earthquake and wind record database

A number of earthquake records of magnitude $5 < M_s < 8$ recorded on alluvium and with distances from geological faults of up to 57 km were downloaded from [7]. These records are assumed to be representative of alluvium and firm soils once it has been shown in [8] that without much variation they would produce similar strength demands to structures located on either soil type. These records have a duration which oscillates between 30 and 80 s and were measured at a time interval of 0.1s. The list of historic earthquake records is provided in Table 1.

Table 1. Synthesised list of earthquake records

| # | Earthquake(s) | Magnitude | Epicentral Distance Km | v_{s30} ms^{-1} | PGA g |
|-------|---|-----------|------------------------|---------------------|-------------|
| 1-2 | Helena Montana-01, 10/31/1935, Carroll College, 180 / 270 | 6 | 2.86 / 2.92 | 593.35/551.82 | 0.16 |
| 3-4 | Northwest Calif-01, 9/12/1938, Ferndale City Hall, 45 / 224 | 5.5 / 5.8 | 53.88 / 53.77 | 219.31 | 0.15 / 0.11 |
| 5-6 | Izmir Turkey, 12/16/1977, Izmir, L / T | 5.3 | 3.21 | 535.24 | 0.42 / 0.13 |
| 7-8 | Dursunbey Turkey, 7/18/1979, Dursunbey, L / T | 5.34 | 9.15 | 585.04 | 0.18 / 0.24 |
| 9-10 | Imperial Valley-02, 5/19/1940, El Centro Array #9, 180 / 270 | 6.95 | 6.09 | 213.44 | 0.25 / 0.15 |
| 11-12 | Northern Calif-01, 10/3/1941, Ferndale City Hall, 225 / 315 | 6.4 | 44.68 | 219.31 | 0.10 / 0.12 |
| 13-14 | Northern Calif-03, 12/21/1954, Ferndale City Hall, 44 / 314 | 6.5 | 27.02 | 219.31 | 0.16 |
| 15 | Borrego Mtn, 4/9/1968, El Centro Array #9, 180 | 6.63 | 45.66 | 213.44 | 0.13 |
| 16-17 | San Fernando, 2/9/1971, Castaic - Old Ridge Route, 21 / 291 | 6.61 | 22.63 | 450.28 | 0.32 / 0.28 |
| 18-19 | San Fernando, 2/9/1971, LA - Hollywood Stor FF, 90 / 180 | 6.61 | 22.77 | 316.46 | 0.22 / 0.16 |
| 20 | San Fernando, 2/9/1971, Lake Hughes #1, 21 | 6.61 | 27.4 | 425.34 | 0.15 |
| 21-22 | San Fernando, 2/9/1971, Lake Hughes #12, 21 / 291 | 6.61 | 19.3 | 602.1 | 0.38 / 0.28 |
| 23-24 | Imperial Valley-06, 10/15/1979, Bonds Corner, 140 / 230 | 6.53 | 2.66 | 223.03 | 0.52 / 0.77 |
| 25-26 | Imperial Valley-06, 10/15/1979, El Centro Array #4, 140 | 6.53 | 7.05 | 208.91 | 0.48 / 0.27 |
| 27-28 | Imperial Valley-06, 10/15/1979, El Centro Array #5, 140 / 230 | 6.53 | 3.95 | 205.63 | 0.33 / 0.38 |
| 29-30 | Imperial Valley-06, 10/15/1979, El Centro Array #7, 140 / 230 | 6.53 | 0.56 | 210.51 | 0.34 / 0.47 |
| 31-32 | Kern County, 7/21/1952, Taft Lincoln School, 21 / 111 | 7.36 | 38.89 | 385.43 | 0.14 / 0.15 |
| 33-34 | Taiwan SMART1(45), 11/14/1986, SMART1 C00, EW / NS | 7.3 | 56.01 | 309.41 | 0.12 / 0.15 |
| 35-36 | Taiwan SMART1(45), 11/14/1986, SMART1 O02, EW / NS | 7.3 | 57.13 | 285.09 | 0.16 / 0.24 |
| 37-38 | Cape Mendocino, 4/25/1992, Petrolia, 0 / 90 | 7.01 | 8.18 | 422.17 | 0.58 / 0.66 |
| 39-40 | Landers, 6/28/1992, Lucerne, 260 / 345 | 7.28 | 2.19 | 1369 | 0.65 / 0.61 |

On the other hand, the wind record database is based on the simulation carried out in [9] which follows the conditional simulation method proposed in [10]. The simulation algorithm requires knowledge of recorded data in at least two points within the region of interest and enables inferring properly correlated wind data series at intermediate points. The two initial data series were calculated by using classical Monte Carlo techniques whereas

intermediate points were calculated at 11 stations covering 250 m along a vertical axis. The mean velocity and turbulence intensity - defined as the ratio between the standard deviation and the mean (σ/\bar{U}), are shown for each simulation point in Table 2 for the case in which $\bar{U} = 20 \text{ ms}^{-1}$. This table also shows how simulated and theoretical first and second-order statistics compare.

Table 2. Calculated statistics of simulated wind time series

| Stats \ z (m) | 10 | 40 | 75 | 100 | 140 | 170 | 200 | 210 | 220 | 240 | 250 |
|---------------|-------|-------|-------|-------|-------|-------|-------|-------|-------|-------|-------|
| \bar{U}_t | 20.00 | 30.21 | 36.21 | 39.79 | 42.95 | 45.39 | 47.77 | 48.52 | 49.15 | 50.18 | 50.87 |
| \bar{U}_s | 19.86 | 29.88 | 35.14 | 38.62 | 41.69 | 44.05 | 46.32 | 47.07 | 47.69 | 48.69 | 49.35 |
| $I_{u,t}$ | 0.295 | 0.206 | 0.244 | 0.221 | 0.195 | 0.172 | 0.146 | 0.137 | 0.130 | 0.116 | 0.107 |
| $I_{u,s}$ | 0.295 | 0.206 | 0.173 | 0.153 | 0.135 | 0.122 | 0.108 | 0.104 | 0.100 | 0.093 | 0.088 |

The reader is referred to [9] for full details of the simulation results.

3. Generalised forces acting on wind turbines and related dynamic effects

Three wind turbine towers of 150 m, 200 m and 250 m height were identified. These are made of steel and have variable section across their length. The towers are assumed to be made of steel with specific weight of 7850 kgm^{-3} , Young's modulus of $200 \times 10^3 \text{ Nm}^{-2}$, damping level of 5%, and are fixed at the base. The geometry and natural vibration frequency of each tower is presented in Table 3.

Table 3. Geometry and natural frequency of wind turbines

| ID # | Height (m) | D_{base} (m) | D_{top} (m) | t_{base} (m) | t_{top} (m) | n_0 (Hz) |
|------|------------|----------------|---------------|----------------|---------------|------------|
| 1 | 150 | 7.5 | 4.0 | 0.05 | 0.016 | 0.44 |
| 2 | 200 | 10 | 7.5 | 0.075 | 0.018 | 0.34 |
| 3 | 250 | 15 | 10 | 0.10 | 0.025 | 0.24 |

Earthquake forces (F_{EQ}) were obtained by multiplying the ground accelerations by the mass of the corresponding segment whilst wind forces (F_W) were estimated through Bernoulli's principle which states $F_W = 1/2 \rho C_D A \bar{U}^2$ - where ρ is the density of the air, C_D is a drag coefficient (taken as 1.4), and A is the area of the segment exposed to wind. Following, generalized forces, F_{EQ}^* and F_W^* , were calculated by using Eq. (1). In this equation $Y^*(z)$ represents force or structural mass per unit length, z is a vertical coordinate, and ϕ is the fundamental modal shape which was approximated by $\phi(z) = (z/H)^\beta$ - with $\beta = 1.5$ and taking H as the height of the tower. The generalised stiffness was obtained with $K^* = 4\pi^2 n_0^2 M^*$, as in [11].

$$Y^* = \int_0^H \phi(z)^2 \Upsilon(z) dz \quad (1)$$

Following, generalised forces were combined in order to find the total force acting on the wind turbines. This is presented in Table 4 for seven levels of wind i.e. including the case in which \bar{U} equals zero, and includes the estimated average ratio F_{EQ}^*/F_W^* . It can be seen in the table that earthquake loading dominates for low values of wind speed whilst peak generalized forces are within similar ranges when $\bar{U} = 10 \text{ ms}^{-1}$. As the wind speed increases the earthquake load loose significance as it can be up to 12% of the wind load (peak values).

Table 4. Total generalized forces ($F_{EQ}^* + F_W^*$) acting on wind turbine towers (kN)

| \bar{U} ms ⁻¹ | H = 150 m | | | H = 200 m | | | H = 250 m | | | Average F_{EQ}^* / F_W^* | | |
|-------------------------------|-----------|------|------|-----------|------|------|-----------|------|------|----------------------------|------|------|
| | mean | rms | peak | mean | rms | peak | mean | rms | peak | mean | rms | peak |
| zero | 0.11 | 9.78 | 92.5 | 0.29 | 30.8 | 284 | 0.78 | 70.8 | 652 | - | - | - |
| 0.5 | 0.39 | 9.79 | 92.6 | 0.95 | 26.3 | 249 | 1.82 | 60.2 | 572 | 10.8 | 167 | 193 |
| 2.5 | 9.08 | 9.97 | 96.1 | 22.1 | 26.7 | 256 | 41.8 | 60.9 | 584 | 0.43 | 6.68 | 7.72 |
| 5 | 36.3 | 12 | 118 | 88.3 | 30.9 | 304 | 167 | 66.9 | 667 | 0.11 | 1.67 | 1.93 |
| 10 | 145 | 28 | 234 | 353 | 64.9 | 570 | 667 | 120 | 1137 | 0.03 | 0.42 | 0.48 |
| 15 | 326 | 58 | 471 | 794 | 133 | 1139 | 1500 | 235 | 2150 | 0.01 | 0.19 | 0.21 |
| 20 | 580 | 101 | 822 | 1411 | 232 | 1987 | 2666 | 405 | 3712 | 0.01 | 0.10 | 0.12 |

The total generalised forces reported in Table 4 were used to determine the dynamic response of the wind turbines. This was done through the numerical integration of Eq. (2) whose explicit solution is given by Eq. (3).

$$m\ddot{d} + c\dot{d} + kd = p(t) \tag{2}$$

$$d(t) = e^{-\xi\omega\Delta t} \left[\left(d(0) - \frac{p_i}{k} + \frac{2s\xi}{\omega_n k} \right) \cos(\omega_D\Delta t) + \left(\dot{d}(0) + d(0)\xi\omega_n - \frac{p_i\xi\omega_n}{k} + \frac{2s\xi^2}{k} - \frac{s}{k} \right) \frac{\sin(\omega_D\Delta t)}{\omega_D} \right] \frac{p_i}{k} + \frac{s\Delta t}{k} - \frac{2s\xi}{\omega_n k} \tag{3}$$

The results of this analysis are shown in Table 5

Table 5. Dynamic response amplitudes (m) calculated for wind turbine towers

| \bar{U} ms ⁻¹ | H = 150 m | | | H = 200 m | | | H = 250 m | | |
|-------------------------------|-----------------------|-------|-------|-----------------------|-------|-------|-----------------------|-------|-------|
| | mean | rms | peak | mean | rms | peak | mean | rms | peak |
| zero | 9.3x10 ⁻⁶ | 0.003 | 0.014 | 2.5 x10 ⁻⁵ | 0.005 | 0.017 | 2.6 x10 ⁻⁵ | 0.006 | 0.021 |
| 0.5 | 1.4 x10 ⁻⁴ | 0.003 | 0.015 | 2.2 x10 ⁻⁴ | 0.005 | 0.022 | 3.6 x10 ⁻⁴ | 0.007 | 0.026 |
| 2.5 | 0.003 | 0.004 | 0.017 | 0.005 | 0.006 | 0.023 | 0.009 | 0.009 | 0.029 |
| 5 | 0.013 | 0.006 | 0.030 | 0.021 | 0.009 | 0.046 | 0.034 | 0.015 | 0.067 |
| 10 | 0.051 | 0.016 | 0.090 | 0.083 | 0.030 | 0.155 | 0.137 | 0.046 | 0.229 |
| 15 | 0.116 | 0.035 | 0.197 | 0.187 | 0.067 | 0.342 | 0.309 | 0.101 | 0.507 |
| 20 | 0.205 | 0.061 | 0.349 | 0.333 | 0.119 | 0.605 | 0.549 | 0.179 | 0.898 |

Table 5 shows a considerable increase of peak displacements for relatively low levels of wind acting on earthquake-resisting structures. For example, when $\bar{U} = 2.5 \text{ ms}^{-1}$ the estimated increase is of 21%, 35%, and 38% on the towers of 150 m, 200 m, and 250 m tall, respectively, whereas when $\bar{U} = 5 \text{ ms}^{-1}$ those figures become 114%, 170%, and 219%. This suggests that the combined effect of earthquake and wind load can be significantly higher than those due to earthquakes only, even for relatively low levels of wind. However, infrastructure could also be designed to withstand wind load only in which case earthquake load would have different levels of impact depending on the design wind load, as suggested by the peak average ratio F_{EQ}^* / F_W^* presented in Table 4.

4. Probabilities associated to wind load in the context of an earthquake event

4.1. Earthquake load as leading accidental action

This section outlines the probabilities associated to the exceedance of three levels of wind speed namely $\bar{U} = 2.5, 5, 10 \text{ ms}^{-1}$. These are identified as the most likely to occur during earthquake events whilst, according to Table 4, would induce critical multi-load scenarios to wind turbines. The probability of occurrence of wind speed is derived from the Weibull distribution function whose general form is given in Eq. (4) In this equation the constants k and c

are the shape and scale parameter respectively, which vary from place to place as these are linked to local conditions such as latitude, orography, soil roughness and seasonal effects.

$$P(\bar{U}) = \frac{k}{c} \left(\frac{\bar{U}}{c}\right)^{k-1} e^{-\left(\frac{\bar{U}}{c}\right)^k} \tag{4}$$

For a particular place, specific values of k and c would be required. However, is possible to establish intervals of these parameters which are commonly seen during full-scale measurements taken across a variety of terrains – see for example those reported in [12-14]. The selected intervals are therefore $2.5 \leq k \leq 4.5$ and $2 \leq c \leq 8$ which derive on probability distribution curves such as those shown in Fig. 1.

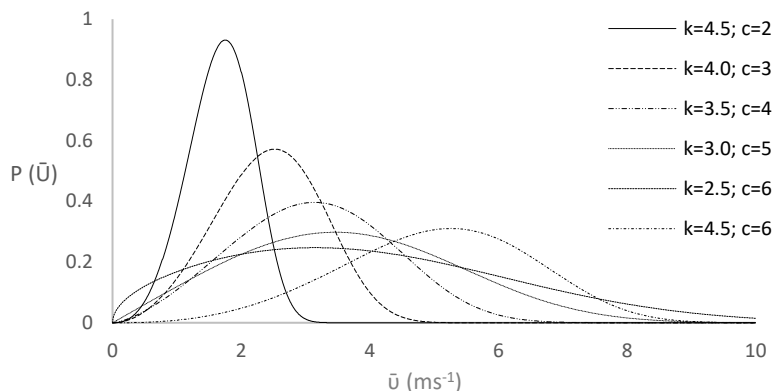


Fig. 1 Weibull distribution of wind under normal conditions

The percentage of time that each one of the selected wind speeds is exceeded was calculated by integrating Eq. (4). The results of this are shown in Table 5 for various combinations of the Weibull parameters.

Table 5. Percentage of time that the target velocity (\bar{U}_{target}) is exceeded.

| k | \bar{U}_{target} (ms ⁻¹) | c | | | | | | |
|-----|--|-------|-------|-------|-------|-------|-------|-------|
| | | 2 | 3 | 4 | 5 | 6 | 7 | 8 |
| 2 | 2.5 | 20.96 | 49.94 | 67.66 | 77.88 | 84.06 | 88.02 | 90.68 |
| | 5 | 0.19 | 6.22 | 20.96 | 36.79 | 49.93 | 60.03 | 67.60 |
| | 10 | 0.00 | 0.00 | 0.19 | 1.83 | 6.22 | 12.97 | 20.81 |
| 2.5 | 2.5 | 17.43 | 53.05 | 73.43 | 83.80 | 89.40 | 92.66 | 94.69 |
| | 5 | 0.01 | 2.77 | 17.43 | 36.79 | 53.05 | 64.97 | 73.43 |
| | 10 | 0.00 | 0.00 | 0.01 | 0.35 | 2.77 | 8.72 | 17.43 |
| 3 | 2.5 | 14.18 | 56.06 | 78.34 | 88.25 | 93.02 | 95.55 | 96.99 |
| | 5 | 0.00 | 0.98 | 14.18 | 36.79 | 56.06 | 69.46 | 78.34 |
| | 10 | 0.00 | 0.00 | 0.00 | 0.03 | 0.98 | 5.42 | 14.18 |
| 3.5 | 2.5 | 11.26 | 58.96 | 82.45 | 91.54 | 95.44 | 97.31 | 98.31 |
| | 5 | 0.00 | 0.25 | 11.26 | 36.79 | 58.96 | 73.49 | 82.45 |
| | 10 | 0.00 | 0.00 | 0.00 | 0.00 | 0.25 | 3.07 | 11.26 |
| 4 | 2.5 | 8.70 | 61.74 | 85.85 | 93.94 | 97.03 | 98.39 | 99.05 |
| | 5 | 0.00 | 0.04 | 8.70 | 36.79 | 61.74 | 77.08 | 85.85 |
| | 10 | 0.00 | 0.00 | 0.00 | 0.00 | 0.04 | 1.55 | 8.70 |
| 4.5 | 2.5 | 6.52 | 64.39 | 88.64 | 95.68 | 98.07 | 99.03 | 99.47 |
| | 5 | 0.00 | 0.00 | 6.52 | 36.79 | 64.39 | 80.25 | 88.64 |
| | 10 | 0.00 | 0.00 | 0.00 | 0.00 | 0.00 | 0.69 | 6.52 |

It is seen in Table 5 that the percentage of time that the target velocity is exceeded increases with the value of c . This in turn makes the range of velocities covered by the Weibull distribution to increase hence allowing area under

the curve defined by Eq. (4) to move right, leaving for example P [$\bar{U} \leq 2.5 \text{ ms}^{-1}$] with a lower value as c tend to 8. This effect can also be inferred through inspection of Fig. 1. On the other hand, it is shown above that the ductility demand on the towers exceeds 20% when $\bar{U} = 2.5 \text{ ms}^{-1}$ with respect to that estimated for the zero-wind load condition, whilst that threshold increase to values over 100% when $\bar{U} = 5 \text{ ms}^{-1}$ - and evidently beyond that when $\bar{U} = 10 \text{ ms}^{-1}$. Furthermore, Table 5 shows that $\bar{U} = 2.5, 5, 10 \text{ ms}^{-1}$ would respectively be exceeded in as much as 99.5%, 88.64% and 20.81% of the time when $c = 8$ and less critically, but still during considerable time frames, for other combinations of k and c .

4.2. Wind load as leading accidental action

Wind turbines which are primarily designed to withstand wind loading would experience considerable increase ductility and strength demands when taking into account earthquake effects. The estimated peak ratio F_{EQ}^* / F_W^* shown in Table 4 is of about 50% when $\bar{U} = 10 \text{ ms}^{-1}$ whilst earthquake loading would represent about 12% of the wind load when $\bar{U} = 20 \text{ ms}^{-1}$. As a consequence, wind turbines designed by considering wind load only would be subject to important transient loading during earthquake events which could make more critical hysteretic effects such as fatigue derived from the tower's dynamic performance. These load combinations would also increase of net forces acting on structural parts and their connections hence additional strength demands to foundations.

5. Final remarks

The variability of multi-load scenarios and their effects on infrastructure has been explained in the context of clean energy generation. It is shown that current design assumptions which disregard the combined effect of earthquake and wind load leave a number of open questions regarding disaster preparedness, prevention and control. Further avenues of research could be identified to help us understand and quantify the consequences of natural phenomena acting as joint events and perhaps to produce more robust design methodologies to mitigate risks.

References

- [1] CATDAT Damage Earthquake Database [Last update 12 May 2014]
- [2] Amos J, 2015. Unsettled earth continues to rattle Nepal. BBC News -12 May 2015
- [3] Shankar Sneha, 2016. Ecuador earthquake: death toll soars, aftershocks reported. International Business Times – 18 April 2016
- [4] Martinez-Vazquez P, 2016. Strength reduction factors for wind and earthquake effects. Building and Structures
- [5] Kiyomiya O, Rikiyi T, Van Gelder H A J M, 2002. Dynamic response analysis of onshore wind energy power units during earthquakes and wind. Twelfth International Offshore and Polar Engineering Conference. Kitakyushu, Japan, May 26-31
- [6] Díaz O, Suárez L E, 2014. Seismic analysis of wind turbines. Earthquake Spectra, 30(2): 743-765
- [7] Pacific Earthquake Engineering Research Centre (PEER). PEER ground motion database <http://ngawest2.berkeley.edu/#disclaimer> [accessed on 19.03.2016]
- [8] Miranda E, 1993. Site-dependent strength reduction factors. J Struct. Eng. ASCE, 119(5): 1319-1338
- [9] Martinez-Vazquez P, Rodriguez-Cuevas N, 2007. Wind field reproduction using neural networks and conditional simulation. Engineering Structures 29: 1442-1449
- [10] Vanmarcke E, Heredia-Zavoni E, Fenton G, 1993. Conditional simulation of spatially correlated ground motion. J. Eng. Mech. 119(11): 2333-2352
- [11] Martinez-Vazquez P, 2016. Strength reduction factors for the combined action of wind and earthquakes. Structures and Buildings. In Press.
- [12] Van Donk S J, Wagner L E, Skidmore L, Tatarko J, 2005. Comparison of the Weibull model with measured wind speed distributions for stochastic wind generation. American Soc. Agricultural Eng. 48(2): 503-510.
- [13] Waewsak J, Chancham C, Landry M, Gagnon Y, 2011. An analysis of wind speed distribution at Thasala, Nahkohn Si Thammaray, Thailand. J. Sustainable Energy & Environment. 2: 51-55.
- [14] Azad A K, Rasul M G, Yusaf T, 2014. Statistical diagnosis of the best Weibull methods for wind power assessment for agricultural applications. Energies. 7: 3056-3085.